Ultrasound Measurement of Vascular Density to Evaluate Response to Anti-Angiogenic Therapy in Renal Cell Carcinoma

Juan D. Rojas, *Student Member, IEEE*, Virginie Papadopoulou, *Member, IEEE*, Tomasz J. Czernuszewicz, Rajalekha M. Rajamahendiran, Anna Chytil, Yun-Chen Chiang, Diana C. Chong, Victoria L. Bautch, W. Kimryn Rathmell, Stephen Aylward, Ryan C. Gessner, and Paul A. Dayton, *Senior Member, IEEE*

Abstract*—*Background: **Functional and molecular changes often precede gross anatomical changes, so early assessment of a tumor's functional and molecular response to therapy can help reduce a patient's exposure to the side effects of ineffective chemotherapeutics or other treatment strategies.** ***Objective:*** **Our intent was to test the hypothesis that an ultrasound microvascular imaging approach might provide indications of response to therapy prior to assessment of tumor size.** ***Methods:*** **Mice bearing clear-cell renal cell carcinoma xenograft tumors were treated with antiangiogenic and Notch inhibition therapies. An ultrasound measurement of microvascular density was used to serially track the tumor response to therapy.** ***Results:*** **Data indicated that ultrasound-derived microvascular density can indicate response to therapy a week prior to changes in tumor volume and is strongly correlated with physiological characteristics of the tumors as measured by histology ($\rho = 0.75$). Furthermore, data demonstrated that ultrasound measurements of vascular density can determine response to therapy and classify between-treatment groups with high sensitivity and specificity.** ***Conclusion/Significance:*** **Results suggests that future applications utilizing ultrasound imaging to monitor tumor response to therapy may be able to provide earlier insight into tumor behavior from metrics of microvascular density rather than anatomical tumor size measurements.**

***Index Terms*—Microvasculature, angiogenesis, ultrasound, contrast agents, response to therapy, acoustic angiography.**

Manuscript received March 6, 2018; revised July 10, 2018; accepted July 18, 2018. Date of publication July 27, 2018; date of current version February 18, 2019. This work was supported in part by the National Institutes of Health under Grants R21CA184387, R44CA165621, R01CA170665, and F31CA196216, and in part by the pilot funding from the University of North Carolina Lineberger Comprehensive Cancer Center. *(Corresponding author: Paul A. Dayton.)*

J. D. Rojas was with the University of North Carolina and North Carolina State University Joint Department of Biomedical Engineering. He is now with SonoVol, Inc.

V. Papadopoulou is with the University of North Carolina and North Carolina State University Joint Department of Biomedical Engineering.

T. J. Czernuszewicz, R. M. Rajamahendiran, and R. C. Gessner are with SonoVol, Inc.

A. Chytil and W. K. Rathmell are with the Department of Medicine, Division of Hematology and Oncology, Vanderbilt University Medical Center.

Y.-C. Chiang was with the University of North Carolina Lineberger Comprehensive Cancer Center. She is now with Novella Clinical.

D. C. Chong was with the University of North Carolina Curriculum in Genetics and Molecular Biology. She is now with Duke University.

V. L. Bautch is with the University of North Carolina Lineberger Comprehensive Cancer Center, Curriculum in Genetics and Molecular Biology, and Department of Biology.

S. Aylward is with Kitware, Inc.

P. A. Dayton is with the University of North Carolina and North Carolina State University Joint Department of Biomedical Engineering, Chapel Hill, NC 27599 USA (e-mail: padayton@email.unc.edu).

Digital Object Identifier 10.1109/TBME.2018.2860932

I. Introduction

THE clinical gold standard in oncology for noninvasively assessing tumor response to therapy is measuring changes in tumor volume via the Response Evaluation Criteria in Solid Tumors (RECIST) [1]. However, functional and molecular changes can occur before any measurable change in tumor size. RECIST may not appropriately demonstrate the effect of therapy [2]–[6], so it is important to closely track both functional and anatomical changes in tumors to more quickly and accurately predict resistance or recurrence, and to tailor treatment for higher efficacy. In particular, previous work has shown that imaging techniques such as contrast-enhanced MRI, perfusion CT, and PET can predict response to antiangiogenic therapies earlier and track it more accurately than RECIST [2], [7]–[12]; however, exposure to radiation from CT and PET, and the cost and long imaging time of MRI, prevent these modalities from being ideal for serial imaging and therapy management.

Compared to MRI, CT, and PET, ultrasound is portable, inexpensive, fast, and does not expose patients to ionizing radiation. Furthermore, Contrast-Enhanced Ultrasound (CEUS) is widely available and uses microbubble contrast agents (MCAs), which are safe for patients and have been used for perfusion and molecular imaging of cancer in the clinic [13]–[16]. CEUS can provide quantitative measures of blood flow [17]–[19] and the expression of different biomarkers [20]–[24]. Additionally, studies in the past several years have shown that CEUS can indicate response and non-response to therapy before changes in tumor volume [25]–[27] and detect response to therapy before measurable differences in tumor volume in rodents with a range of tumor types [28]–[34] and in human patients [35]. This is of particular interest since the ability to closely track disease progression may allow clinicians to tailor treatments for improved efficacy.

Acoustic Angiography (AA) is another CEUS technique which uses the super-harmonic signals from MCAs to produce high-resolution maps of vasculature [36], [37]. AA takes advantage of the fact that tissue does not produce super harmonic signals to generate images of vasculature with very high contrast-to-tissue ratios that cannot be achieved with other CEUS techniques. Furthermore, AA can provide quantitative measurements of vascular density, blood perfusion, and vessel morphology [38]–[40]. Many studies have shown that CEUS can be used to accurately track and predict response to therapy for treatment groups. Here, we use AA to predict response to therapy before measurable changes in tumor volume for individual cases with high sensitivity and specificity.

A common clinical therapeutic strategy for the treatment of cancer is antiangiogenic treatment [4], [41]–[44]. Drugs such as Sunitinib, a small molecule multi-kinase inhibitor, reduces the signaling of the Vascular Endothelial Growth Factor (VEGF) pathway via its receptor VEGFR-2 [4], [41]–[44]. The VEGF pathway plays a key role in tumor angiogenesis, such that inhibition reduces new vessel formation and starves the tumor. Antiangiogenic therapy is initially effective against clear-cell Renal Cell Carcinoma (ccRCC), which is characterized by increased angiogenesis [45], [46], although resistance to antiangiogenic therapy is almost universally developed after several months of therapy [47]–[49]. Inhibition of the Notch signaling pathway is an alternative strategy to antiangiogenic therapy that also impairs angiogenesis. Notch signaling promotes vessel growth while suppressing excessive sprouting by down regulating VEGFR-2 [50]–[52]. Thus, inhibiting Notch signaling produces aberrant sprouting of immature vasculature and has been shown to inhibit tumor growth [51], [53]–[56]. These complementing inhibitory pathways provide an opportunity for parallel angiogenic blockade, and moreover, the additional expression of VEGFR-2 caused by the inhibition of Notch may cause this strategy to be synergistic with VEGFR-2 inhibition.

In this work, we hypothesize that vascular density assessment from AA imaging is related to tumor progression and can predict response to antiangiogenic and Notch inhibition therapies earlier than conventional measurements of tumor volumetric changes. Additionally, we compare the imaging-derived metrics for tumor response to histologically derived measurements of blood vessel density and show they produce physiologically relevant information about tumor vasculature. Finally, we show that vascular density from AA can predict response to therapy with high sensitivity and specificity.

II. Methods

A. Contrast Agent Formulation

The lipid-encapsulated perfluorocarbon MCAs used in this work were manufactured in-house and were similar to commercial lipid-shelled contrast agents. The lipids 1,2-distearoyl-sn-glycero-3-phosphocholine and 1,2-distearoyl-sn-glycero-3-phosphoethanolamine-N-methoxy (polyethylene-glycol)-2000 (DSPE-PEG2000) in a 9:1 M ratio and a total lipid concentration of 1.0 mg/mL were dissolved in a solution of phosphate-buffered saline, propylene glycol, and glycerol (16:3:1). Then, 1.5 mL of the solution was added to a 3-mL glass vial and the head space was gas-exchanged with Decafluorobutane gas. Microbubbles (1 μm mean diameter and a 1×10^{10} #/mL concentration) were produced by using an agitation technique.

B. Xenograft and Treatment Protocol

A total of 32 NSG (NOD/scid/gamma) female mice (Mus musculus) were injected subcutaneously in the flank with 8 $\times$ 106 786-O human ccRCC cells. Mice were initially separated into 4 groups: VEGFR-2 inhibitor SU (Sunitnib malate, Selleckchem, TX, USA), a combination of SU and the Notch pathway inhibitor GSI (Gamma secretase inhibitor, PF-03084014, Pfizer, New York, NY, USA), a Switch group which would be treated with SU and switched to the Combo treatment after 3 weeks, and Control (100 μL of saline). However, it was decided after the start of treatment that the Switch treatment would be explored in a separate larger study, so the Switch mice were added to the SU group and remained on SU treatment. Therefore, the final number of animals in each group were 8, 14, and 7 for the Control, SU, and Combo groups, respectively. The mice in the SU group were administered 50 mg/kg of SU, while the mice in the Combo group were given a combination of 50 mg/kg of SU and 90 mg/kg of GSI by oral gavage. The volume of the tumors was measured using calipers every 2 days and treatment commenced for four weeks once the tumors reached a size of 200 mm^3. Injection, treatment, and imaging protocols were approved by UNC Institutional Animal Care and Use Committee (IACUC).

C. Animal Preparation Protocol and Contrast Administration

Imaging started with a pre-treatment scan once the tumors reached a size of 150 mm^3 and continued once per week until the end of treatment. During each imaging session, the mice were anesthetized with 1.5% isoflurane and warmed with a heat lamp to maintain body temperature. The area around the tumor was shaved using an electric razor and further depilated with a chemical hair remover. A 27-gauge catheter was inserted into the tail vein for the administration of MCAs, which were continuously infused at a rate of 1.5 $\times$ 108 bubbles/min.

D. Imaging System

The imaging system used for this work was a Vega platform (SonoVol, Inc., Research Triangle Park, NC), which allows for automated 3D ultrasound image acquisition from mice. The system was used in both high-frequency/high-resolution B-mode (24 MHz) for anatomical reference and AA mode (transmit 2 MHz with a 1.1 MPa peak-negative pressure, receive 24 MHz) for microvascular analysis. Further details of this system have been previously described in [57].

E. Imaging Protocol

A 3D B-mode "scout scan" with an elevational resolution of 200 μm of was used to locate the tumor. Next, AA images were captured around the tumor location 30 seconds after the start

of the MCA infusion. AA imaging consisted of a continuous sweep acquisition, which produced images of vasculature with an elevational resolution of around 500 μm. The tumor was scanned 16 times, allowing MCAs to reperfuse into the tissue for 10 seconds between each scan, and a final AA image was computed by averaging all the acquisitions.

F. Noninvasive Measurements of Tumor Size and Vascular Density

Tumor ROIs were manually segmented using SonoEQ (SonoVol, Inc., Research Triangle Park, NC) analysis software from B-mode anatomical reference images. Blood vessel density (BVD), or the percentage of the tumor that had measurable perfusion, was computed from the AA microvasculature images by dividing the number of voxels with intensity values higher than a fixed, predetermined threshold by the total number of voxels in the ROI. The tumor volume was calculated by summing the number of voxels inside the ROI and multiplying by the spatial dimensions of a voxel.

G. Organization of Volume and Density Data

The mice started treatment at different days, since the dosing began once the tumors reached 200 mm^3, so that imaging time points for different animals correspond to different days before/after the start of treatment. Therefore, the imaging time points that were captured before the start of treatment were binned into a baseline (-1) week, those that occurred between 1 and 7 days after the start of treatment were binned into week 1 of imaging, 8–14 days into week 2, 15–21 days into week 3, and 22–28 days after the start of treatment into week 4 of imaging.

H. Histological Assessment of Vessel Density

CD31 immunohistochemistry was performed to serve as a gold standard for comparison against imaging results. Tumors were surgically extracted at necropsy, which occurred after the last imaging time point or earlier if the size limit was exceeded. Three tumors from each treatment group were used for the histological analysis, except for the SU group from which 6 tumors were used. Immunohistochemistry was performed on paraffin-embedded tumor sections on a Leica Bond Max auto-stainer using anti-CD31 from Novocastra (cat # NCL-CD31-1A10). Following heat-induced epitope retrieval in EDTA for 20 min, the antibody was incubated on the tissue for 1 h at a dilution of 1:100 then visualized with diaminobenzidine (DAB). Serial stained sections from each treatment group (10 sections per tumor) were digitized by an Olympus DP 72 (Olympus Corporation, Center Valley, PA) or an Infinity2 camera at 200×, and the percentage of positively stained area was determined using ImageJ [58].

I. Statistical Analysis

A right-tailed Spearman test was used to assess the correlation between the last imaging BVD timepoint and histology for different threshold values in order to select the most appropriate threshold. A Kruskal-Wallis analysis with Tukey multiple comparison post-test was performed to determine if the BVD or volume were significantly different between the treatment groups over the time-course of the study. Significance was set at $p < 0.05$.

Furthermore, the BVD at early time points was used to predict response to treatment (treated vs untreated, inferred from the tumor volume at later time points). The BVD around day 7 (day 6 to 10) after the start of treatment was plotted against the corresponding tumor volume measurements from around day 21 (day 17 to 24). A linear regression model was used to fit the data, so that a predicted tumor volume (PTV) for each animal could be calculated from the BVD around day 7. Next, PTV values above and below a threshold were classified as untreated or treated, respectively, for a range of thresholds. Using receiver-operator curve (ROC) analysis, the PTV threshold that produced the best sensitivity (true positive) and specificity (true negative) at separating treated and untreated was calculated.

III. Results

Fig. 1 shows representative BVD images for each treatment group before the start of treatment and at the end of the study. At the pretreatment time-point, all tumors were well perfused (blue line indicates boundary, yellow indicates MCA). Over the duration of the study, untreated tumors in the control group (top row) exhibited continued growth without significant vascular changes, while the SU and Combo treated tumors (middle and bottom row, respectively) saw stunted growth and a marked decrease in MCA signal density and intensity, indicating vascular disruption.

Due to unknown health issues, tumor size limitations, and inability to insert the catheter into the tail vein for contrast administration, the different imaging weeks had varying numbers of mice (Table I). Only control animals were sacrificed because of tumor burden, and euthanasia was the only reason for the decrease in group size, except for one catheter failure on week 2. For the treatment groups, 6 SU and 3 Combo mice died before the end of treatment, and some mice were not imaged because they were not stable under anesthesia or a catheter could not be inserted into the tail vein (also likely due in part to therapy side-effects including dehydration and weight loss). This resulted in all the Combo and Control mice, and 86% (on average) of the SU mice that were still alive to be imaged at each timepoint.

A. Assessing Response to Therapy

Quantitative assessment of tumor response to therapy is depicted in Fig. 2. The BVD for the Combo and SU groups were significantly lower ($p < 0.05$) from the Control after only a week of treatment, while it took 2 weeks for the volumes to become significantly different between the groups (Fig. 2). The BVD for the Combo group remained significantly lower from that of the Controls for the remainder of the study, and although the SU group had a lower median BVD value than the Control group, the difference was not statistically significant after the first week of treatment.

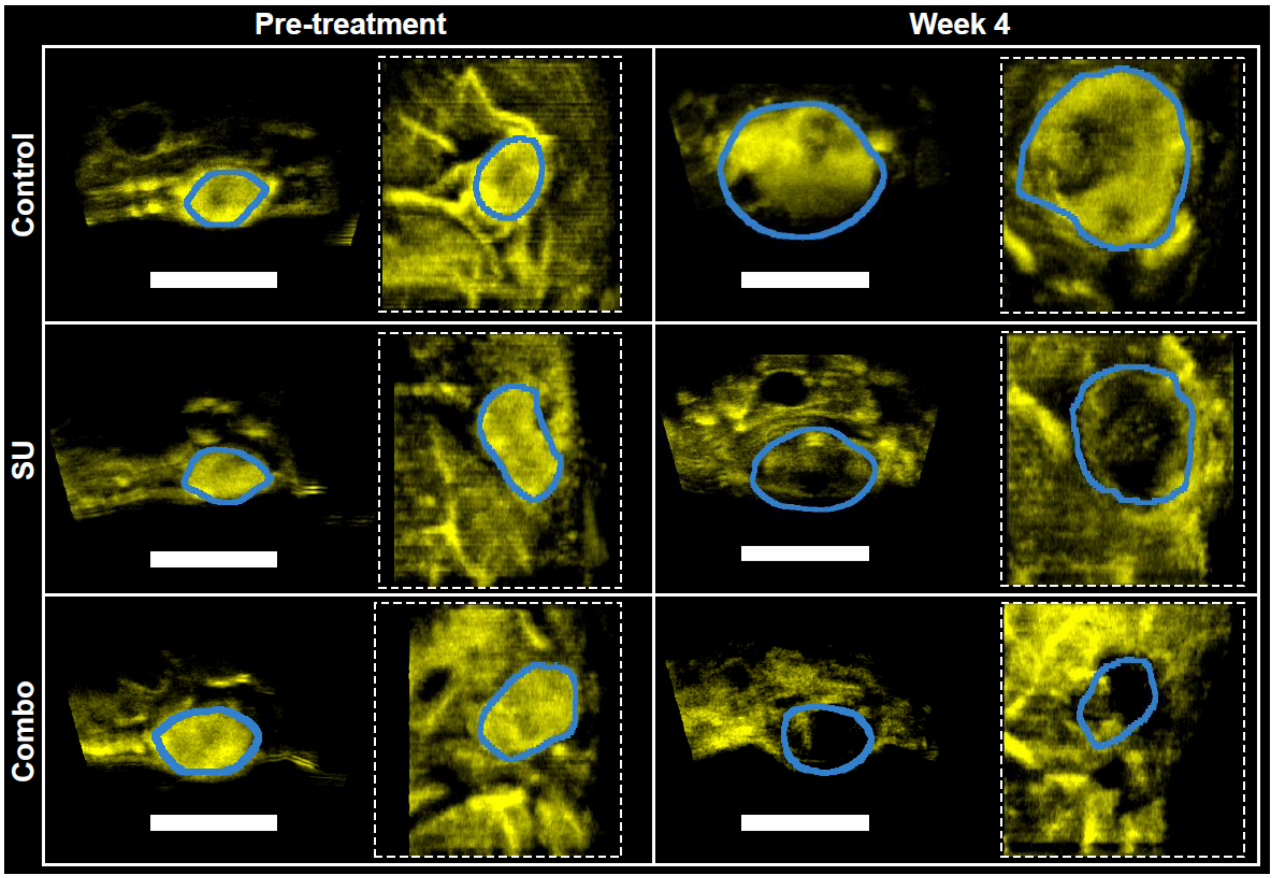

Fig. 1. Representative vessel density images from the different treatment groups. Representative images are displayed at the beginning (left) and end (right) of the study. In each panel, the image on the left is a cross-section of the tumors while the image on the right (dashed square) is a coronal view. The scale bar represents 1 cm. Yellow indicates microvasculature acquired in AA mode. The blue outlines the tumor region of interest, and was derived via registered anatomical B-mode images (not shown).

TABLE I
NUMBER OF ANIMALS IMAGED FOR EACH TREATMENT WEEK

	Imaging Week				
	-1	*1*	*2*	*3*	*4*
Control	8	8	6	6	4
SU	12	10	11	12	8
Combo	6	6	5	6	4

B. Using Volume and Density for Classification of Treatment

The volume measurements of all mice at every imaging time point after the start of treatment were plotted against the corresponding BVD values (Fig. 3), and a line with a fixed y-intercept was used to classify the data points as treated (under line) or untreated (above line). Using the slope as a classifier, the sensitivity and specificity for a range of slopes were calculated. Setting the slope at $-0.06\%/\text{mm}^3$ (shown in Fig. 3), the sensitivity and specificity were 89% and 92%, respectively, at classifying the control group from the treated groups. Moreover, when the same slope was used to classify the Control group from the SU and Combo groups individually, the sensitivity was 84% and 100% for SU and Combo, respectively.

When only the data from week 1 was used for the analysis (Fig. 3b), the sensitivity and specificity were 84% and 88% when classifying between treated and untreated, and the sensitivity was 75% and 100% for the SU and Combo, respectively, when the Controls were classified against each group individually.

C. Validation of Vessel Density Measurement Using Histology

The histological results collected after 4 weeks of treatment demonstrate that the amount of CD31 neovasculature via staining in the tumors for the SU and Combo groups was significantly lower ($p < 0.05$) than that of the Controls (Fig. 4). The stained area was quantified and compared to the BVD results, and a strong correlation was demonstrated (Fig. 5). Furthermore, the correlation coefficient ρ was similar between the users ($\rho = 0.77 \pm 0.03$). These results confirm that vascular density measurements acquired through AA imaging correlate with histological vascular density measurements.

D. Assessing Response to Treatment

The relationship between BVD around day 7 versus tumor volume around day 21 had a significant correlation ($p < 0.001$) and a spearman coefficient of 0.82 (Fig. 6). An ROC curve

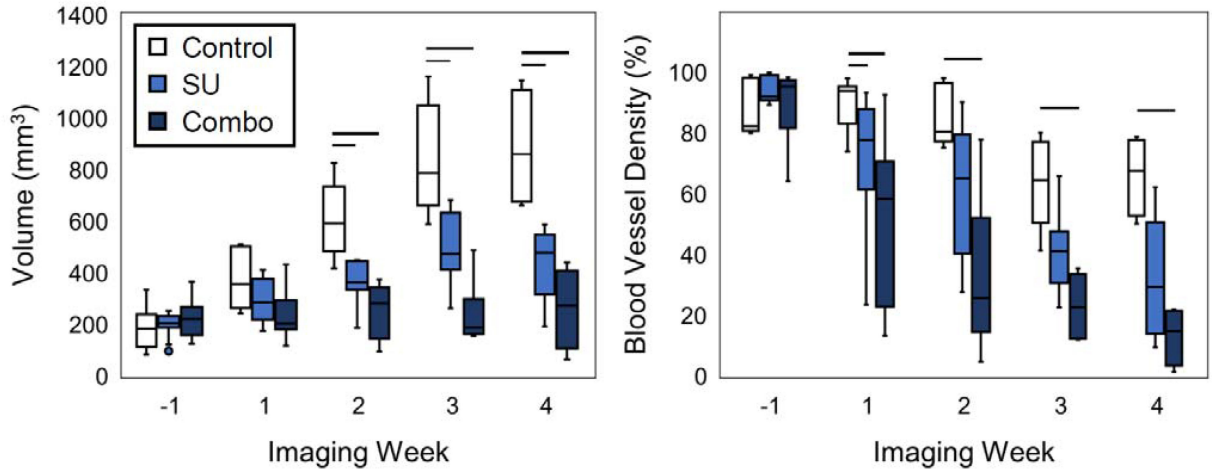

Fig. 2. Tumor volume and blood vessel density for the different imaging weeks. The vessel density (right) of the SU and Combo groups became significant ($p < 0.05$) from the Controls 1 week after the start of treatment, while it took 2 weeks for a significant difference in volume (left) to emerge. Significance is denoted by the horizontal bars.

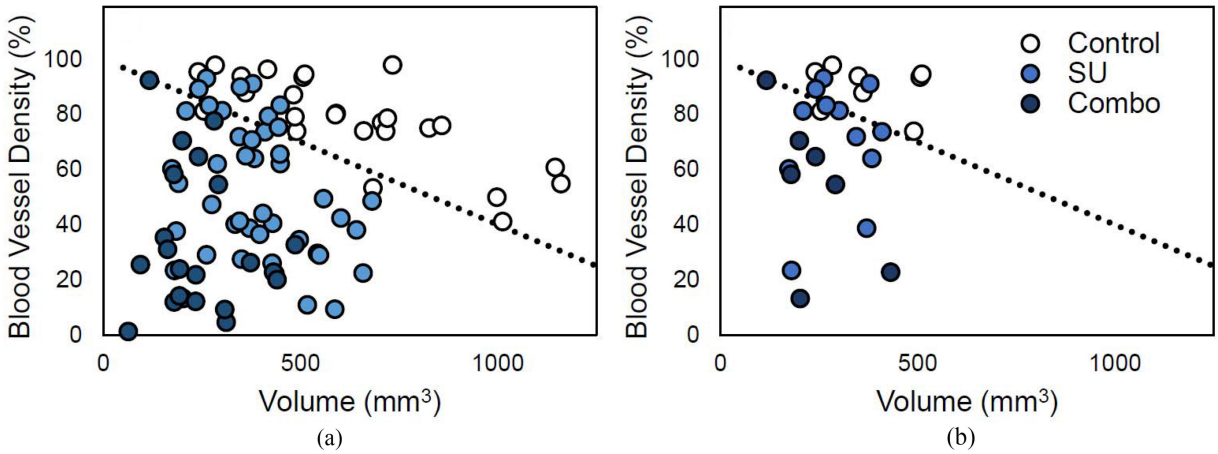

Fig. 3. Plot of BVD vs volume for all datapoints. The two plots display the points after the start of treatment (a) and only those at week 1 (b). A line with a y-intercept set at 100% BVD (black dotted line) can be used to separate the data between treated (under the line) and untreated (above the line).

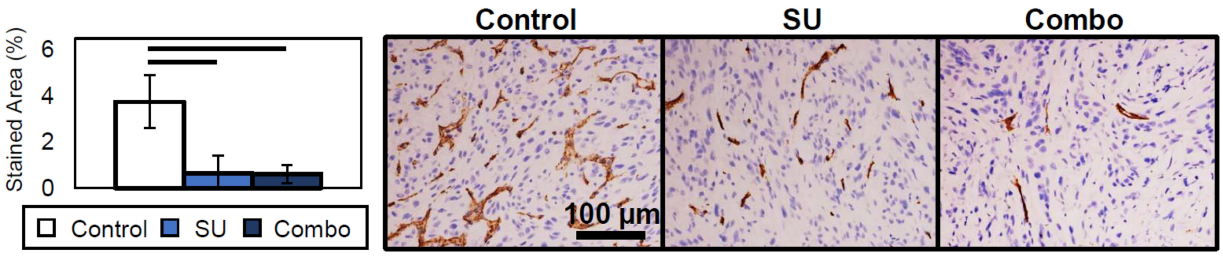

Fig. 4. Representative CD31 staining images of the different treatment groups and Stained Area results. The SU and Combo groups had significant values ($p < 0.05$) from the Control group. SU and Combo groups were not statistically significantly different from each other.

was plotted using different PTV thresholds found using the equation of the linear fit model (Fig. 6a) and the BVD values from around 7 days after the start of treatment (Fig. 6b), and the curve indicates that a maximum sensitivity and specificity of 94% and 86%, respectively, can be obtained when using a PVT threshold value of 705 mm^3. Therefore, the results show that BVD can be used to differentiate between treated and untreated tumors for individual mice with strong confidence.

IV. Discussion

In this work, data supports our hypothesis that BVD derived from microvascular imaging can evaluate tumor response to

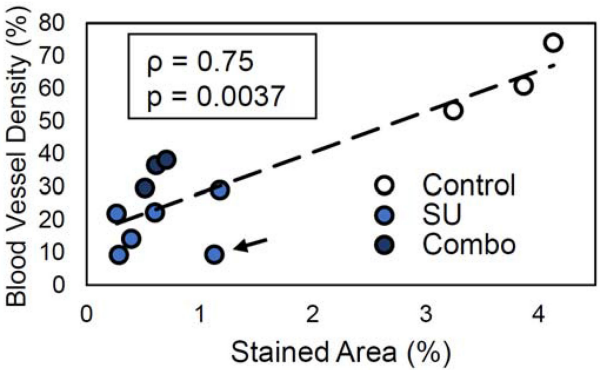

Fig. 5. Correlation plot of image derived blood vessel density (BVD) vs CD31 stained neovasculature. The results show strong correlation ($\rho = 0.75$) between imaging and histology. Dotted line indicates the linear regression line. The black arrow is pointing towards an outlier measurement in the plots that reduces the strength of the correlation.

therapy earlier than conventional tumor volume measurements, in a rodent model of renal cell carcinoma treated with antiangiogenic and Notch inhibition therapies.

It is important to accurately and closely track response to therapy of tumors to minimize undesirable side effects of chemo or radiotherapy if treatment begins to fail. Furthermore, the array of available therapies for ccRCC is expanding rapidly, creating a scenario where selecting therapy for an individual patient will be more relevant than ever. Conventional methods for evaluating response to therapy typically rely on changes of tumor volume, typically at an interval of 3 months, but tracking volume has been shown to be inaccurate and often underreports the effect of therapy. Imaging techniques such as dynamic contrast-enhanced MRI and metabolic PET imaging have been shown to be effective at tracking and predicting response to therapy by providing functional insights rather than simple changes in tumor volume. These modalities are associated with challenges such as lack of bedside support, cost, contrast contraindications (MRI), and requirements for access to short-lived isotopes (PET). In contrast, CEUS is inexpensive, portable, and safe for repeated serial imaging. Here we demonstrate that vascular density measurements from AA correlate well with histology and can detect response to therapy earlier than changes in tumor volume. Admittedly, current AA microvascular imaging is limited to within a few centimeters of depth, and therefore performs best in rodents, however, future advancements may enable this or similar ultrasound microvascular techniques such as super-resolution imaging [59]–[61] for deeper clinical imaging.

The data illustrate that microvascular assessment in conjunction with volume measurements can classify tumors as treated or untreated with very high sensitivity and specificity (Fig. 3). The results suggest that a tumor can be correctly classified a responder to therapy regardless of its size or duration of treatment with a high degree of confidence. Sensitive classification can be accomplished within a week of the start of treatment, which cannot be accomplished with tumor volume measurements alone, and can be beneficial for clinical applications. While the sensitivity of classifying the tumors treated with SU is only about 75% at week one, every tumor treated with the combination therapy was correctly classified at the week 1 time point (Fig. 3). Furthermore, the BVD values from around day 7 can be used to predict treatment response with a high degree of confidence before tumor volume measurements become significantly different (Fig. 6). Although survival outcomes would need to be tracked in order to relate the observed changes in tumor properties to successful or failed treatment, initial results about our ability to assess a tumor's response to treatment compared to controls based on microvascular density prior to volume measurements were encouraging.

Histological validation demonstrated that the relative correlation between image based vascular density and vascular density from histology was high (Fig. 5), but the value ranges of the two metrics were vastly different. The explanation for this discrepancy lies in the resolution of the two techniques. While optical microscopy, which was used for the histological analysis, can resolve individual capillaries, AA ultrasound imaging utilized here will blur any vessels smaller than the resolution of 100–150 μm in diameter into the entire image voxel, indicating a higher vascular density than optical histology analysis.

There was a strong correlation between imaging results and histology ($\rho = 0.75$), however, a single data point indicated by the arrow in Fig. 5 reduces the correlation, and when it is removed from the analysis, ρ is 0.9. This suggests that this point was a substantial outlier, and it is likely that a higher correlation overall may be achieved than reported in this study if a larger data set is utilized.

Surprisingly, only 50% of the mice in the SU and Combo groups survived the entire study (Table I). There is no work reporting this rate of morbidity as a result of the drugs used here, and a recent study using the same tumor model, therapeutics, and dosage demonstrated no negative health effects on the animals [28]. It is unclear what effect the health issues of the mice had on the results of the study, but the findings of this work agree with those of previous studies which used similar treatment strategies [27]–[29], [34]. In addition to the loss of mice due to health issues, the Control mice grew quickly and were euthanized once the tumors reached the size limit so that only ~50% of mice in that group remained at the week 4 time point. Therefore, the diminishing number of mice in the groups probably contributed to the lack of significance in the BVD between the Control and SU groups after the first week of imaging, even though the values appeared to be different (Fig. 7). Another reason why the BVD of the SU and Control groups was not significant at the end of the study, unlike the histological results, is that the binning of data into weeks results in mice that have been treated for varying amounts of time to be grouped into the same week (e.g., 14 days and 20 days were binned into week 2 of treatment), which likely introduced additional variability. Furthermore, while the BVD values being compared for each group was small (around 4 per group) at the last time point, 30 histology images for each group were used for analysis.

Detecting response to therapy using imaging one week earlier than changes in tumor volume does not seem substantial, however, while rodent cancer evolution has a timescale of days to weeks, it takes several weeks to several months to observe response to therapy in humans [2], [9], [62]. Therefore, a difference of a week in mice may translate to more clinically relevant time scales in humans.

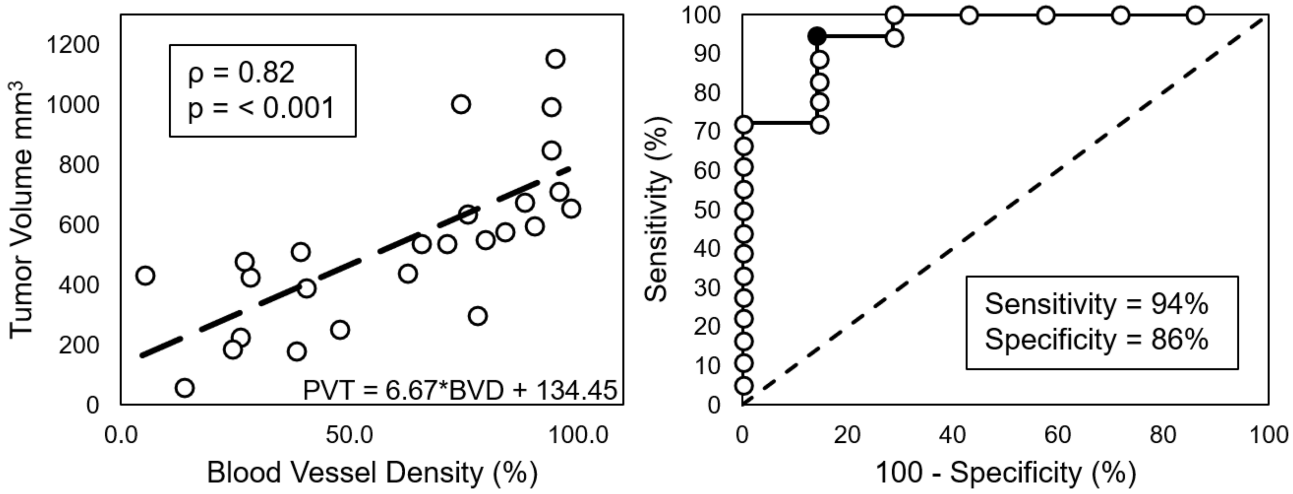

Fig. 6. Linear regression model used to calculate predicted tumor volume (PTV) and ROC curve for PTV as a classifier. Plot (a) shows the linear regression model (dashed black line) of BVD vs tumor volume used to calculate PTV, and plot (b) shows the ROC curve for PTV as a classifier of treated and untreated tumors. the black filled in circle in the ROC curve represents the PTV threshold with the highest sensitivity (94%) and specificity (86%) and corresponds to a value of 705 mm^3. The dashed line in (b) represent a random chance (50%) of correctly classifying the data.

Lastly, the results of this work, and previous work showing that GSI may not be a good treatment alternative [28], demonstrate that a combination of SU and GSI provides a better strategy for angiogenic suppression than delivering either drug individually. The volume results demonstrate that while the SU group had reduced tumor growth from the Controls, the Combo group alone caused the stagnation of tumor growth, and in some cases produced a reduction in tumor volume (Fig. 2).

V. Conclusion

In this work, we demonstrate that an ultrasound metric of vascular density can be used to assess the response of ccRCC tumors to antiangiogenic and Notch inhibition therapies earlier than tumor volume, which is the clinical gold standard. This application of contrast enhanced ultrasound has important merits as a variety of targeted and immunotherapy agents crowd the treatment landscape of ccRCC. Furthermore, the results demonstrate that vessel density measurements can classify between treated and untreated tumors and predict response to therapy early in the treatment with high sensitivity and specificity. Future studies will need to be performed in humans to establish if these findings carry over to a clinical population.

Acknowledgment

The authors appreciate the extensive editing from Dr. Virginie Papadopoulou. They would like to acknowledge the University of North Carolina Animal Core for their help during the imaging experiments and Brian Velasco for providing the lipid solution for the making of the contrast agents used in the study.

Conflicts of Interests: Authors P.A.D. and R.C.G. are inventors on a patent describing Acoustic Angiography and are equity holders in SonoVol, Inc., a company which has licensed this patent, and whose imaging system technology was utilized in this work.

References

[1] P. Therasse *et al.*, "New guidelines to evaluate the response to treatment in solid tumors," *J. Nat. Cancer Inst.*, vol. 87, no. 12, pp. 881–886, 2000.
[2] R. S. Benjamin *et al.*, "We should desist using RECIST, at least in GIST," *J. Clin. Oncology*, vol. 25, no. 13, pp. 1760–1764, 2007.
[3] J. C. Yang *et al.*, "A randomized trial of Bevacizumab, an anti-vasucular endothelial growth factor antibody, for metastatic renal cancer," *New Engl. J. Med.*, vol. 349, no. 5, pp. 427–434, 2003.
[4] B. Escudier *et al.*, "Sorafenib in advanced clear-cell renal-cell carcinoma," *New Engl. J. Med.*, vol. 356, no. 2, pp. 125–134, 2007.
[5] H. Choi *et al.*, "Correlation of computed tomography and positron emission tomography in patients with metastatic gastrointestinal stromal tumor treated at a single institution with imatinib mesylate: Proposal of new computed tomography response criteria," *J. Clin. Oncology*, vol. 25, no. 13, pp. 1753–1759, 2007.
[6] M. Lamuraglia *et al.*, "To predict progression-free survival and overall survival in metastatic renal cancer treated with sorafenib: Pilot study using dynamic contrast-enhanced Doppler ultrasound," *Eur. J. Cancer*, vol. 42, no. 15, pp. 2472–2479, 2006.
[7] B. Morgan *et al.*, "Dynamic contrast-enhanced magnetic resonance imaging as a biomarker for the pharmacological response of PTK787/ZK 222584, an inhibitor of the vascular endothelial growth factor receptor tyrosine kinases, in patients with advanced colorectal cancer and Liv," *J. Clin. Oncology*, vol. 21, pp. 3955–3964, 2003.
[8] H. A. Wieder *et al.*, "Time course of tumor metabolic activity during chemoradiotherapy of esophageal squamous cell carcinoma and response of treatment," *J. Clin. Oncology*, vol. 22, no. 5, pp. 900–908, 2004.
[9] P. D. Nathan *et al.*, "CT response assessment combining reduction in both size and arterial phase density correlates with time to progression in metastatic renal cancer patients treated with targeted therapies," *Cancer Biol. Therapy*, vol. 9, no. 1, pp. 14–19, 2010.
[10] S. Stroobants *et al.*, "18FDG-Positron emission tomography for the early prediction of response in advanced soft tissue sarcoma treated with imatinib mesylate (Glivec)," *Eur. J. Cancer*, vol. 39, no. 14, pp. 2012–2020, 2003.
[11] I. Zerizer *et al.*, "The role of early 18F-FDG PET/CT in prediction of progression-free survival after 90Y radioembolization: Comparison with RECIST and tumour density criteria," *Eur. J. Nucl. Med. Mol. Imag.*, vol. 39, pp. 1391–1399, 2012.
[12] E. Frampas *et al.*, "Advanced hepatocellular carcinoma: Early evaluation of response to targeted therapy and prognostic value of perfusion CT and dynamic contrast enhanced-ultrasound. Preliminary results," *Eur. J. Radiol.*, vol. 82, pp. 205–211, 2013.
[13] K. Cox *et al.*, "Contrast-enhanced ultrasound biopsy of sentinel lymph nodes in patients with breast cancer: Implications for axillary metastases and conservation," *Ann. Surg. Oncology*, vol. 23, no. 1, pp. 58–64, 2016.

[14] S. K. Kasoji *et al.*, "A pilot clinical study in characterization of malignant renal cell carcinoma subtype with contrast-enhanced ultrasound," *Ultrason. Imag.*, vol. 39, no. 2, pp. 126–136, 2016.

[15] J. K. Willmann *et al.*, "Ultrasound molecular imaging with BR55 in patients with breast and ovarian lesions: First-in-human results," *J. Clin. Oncology*, vol. 35, no. 19, pp. 2133–2140, 2017.

[16] M. Smeenge *et al.*, "First-in-human ultrasound molecular imaging with a VEGFR2-specific ultrasound molecular contrast agent (BR55) in prostate cancer," *Investigative Radiol.*, vol. 52, no. 7, pp. 419–427, 2017.

[17] P. Kogan *et al.*, "Validation of dynamic contrast-enhanced ultrasound in rodent kidneys as an absolute quantitative method for measuring blood perfusion," *Ultrasound Med. Biol.*, vol. 37, no. 6, pp. 900–908, Jun. 2011.

[18] V. H. J. Roberts *et al.*, "Quantitative assessment of placental perfusion by contrast-enhanced ultrasound in macaques and human subjects," *Amer. J. Obstetrics Gynecology*, vol. 214, no. 3, pp. 214–369, 2016.

[19] S. Feingold *et al.*, "Quantitative volumetric perfusion mapping of the microvasculature using contrast ultrasound," *Investigative Radiol.*, vol. 45, no. 10, pp. 669–674, 2010.

[20] C. Bachmann *et al.*, "Targeting mucosal addressin cellular adhesion molecule (MAdCAM)-1 to noninvasively image experimental Crohn's disease," *Gastroenterology*, vol. 130, no. 1, pp. 8–16, 2006.

[21] J. L. Tlaxca *et al.*, "Ultrasound-based molecular imaging and specific gene delivery to mesenteric vasculature by endothelial adhesion molecule targeted microbubbles in a mouse model of Crohn's disease," *J. Control. Release*, vol. 165, no. 3, pp. 216–225, 2013.

[22] J. J. Rychak *et al.*, "Microultrasound molecular imaging of vascular endothelial growth factor receptor 2 in a mouse model of tumor angiogenesis," *Mol. Imag.*, vol. 6, no. 5, pp. 289–296, 2007.

[23] J. Bzyl *et al.*, "Molecular and functional ultrasound imaging in differently aggressive breast cancer xenografts using two novel ultrasound contrast agents (BR55 and BR38)," *Eur. Radiol.*, vol. 21, no. 9, pp. 1988–1995, 2011.

[24] I. Leguerney *et al.*, "Molecular ultrasound imaging using contrast agents targeting endoglin, vascular endothelial growth factor receptor 2 and integrin," *Ultrasound Med. Biol.*, vol. 41, no. 1, pp. 197–207, 2015.

[25] J. E. Streeter *et al.*, "A comparative evaluation of ultrasound molecular imaging, perfusion imaging, and volume measurements in evaluating response to therapy in patient-derived xenografts," *Technol. Cancer Res. Treatment*, vol. 12, no. 4, pp. 311–321, 2013.

[26] S. R. Sirsi *et al.*, "Contrast ultrasound imaging for identification of early responder tumor models to anti-angiogenic therapy," *Ultrasound Med. Biol.*, vol. 38, no. 6, pp. 1019–1029, 2012.

[27] J. Zhou *et al.*, "VEGFR2-targeted three-dimensional ultrasound imaging can predict responses to antiangiogenic therapy in preclinical models of colon cancer," *Cancer Res.*, vol. 76, no. 14, pp. 4081–4089, 2016.

[28] J. D. Rojas *et al.*, "Ultrasound molecular imaging of VEGFR-2 in clear-cell renal cell carcinoma tracks disease response to antiangiogenic and Notch-inhibition therapy," *Theranostics*, vol. 8, no. 1, pp. 141–155, 2018.

[29] R. S. Eschbach *et al.*, "Contrast-enhanced ultrasound with VEGFR2-targeted microbubbles for monitoring regorafenib therapy effects in experimental colorectal adenocarcinomas in rats with DCE-MRI and immunohistochemical validation," *PLoS One*, vol. 12, no. 1, pp. 1–22, 2017.

[30] S. C. Baetke *et al.*, "Squamous cell carcinoma xenografts: Use of VEGFR2-targeted microbubbles for combined functional and molecular US to monitor antiangiogenic therapy effects," *Radiology*, vol. 278, no. 2, pp. 430–440, 2016.

[31] H. Wang *et al.*, "Three-dimensional ultrasound molecular imaging of angiogenesis in colon cancer using a clinical matrix array ultrasound transducer," *Investigative Radiol.*, vol. 50, no. 5, pp. 322–329, 2015.

[32] M. A. Pysz *et al.*, "Vascular endothelial growth factor receptor type 2-targeted contrast-enhanced US of pancreatic cancer neovasculature in a genetically engineered mouse model: Potential for earlier detection," *Radiology*, vol. 274, no. 3, pp. 790–799, 2015.

[33] H. Wang *et al.*, "Intra-animal comparison between three-dimensional molecularly targeted US and three-dimensional dynamic contrast-enahnced US for early antiangiogenic treatment assessment in colon cancer," *Radiology*, vol. 282, no. 2, pp. 443–452, 2017.

[34] J. Zhou *et al.*, "Early prediction of tumor response to bevacizumab treatment in murine colon cancer models using three-dimensional dynamic contrast-enhanced ultrasound imaging," *Angiogenesis*, vol. 20, pp. 547–555, 2017.

[35] N. Lassau *et al.*, "Advanced hepatocellular carcinoma: Early evaluation of response to bevacizumab therapy at dynamic contrast-enhanced US with quantification-preliminary results," *Radiology*, vol. 258, no. 1, pp. 291–300, 2011.

[36] R. C. Gessner *et al.*, "Acoustic angiography: A new imaging modality for assessing microvasculature architecture," *Int. J. Biomed. Imag.*, vol. 2013, 2013, Art. no. 936593.

[37] R. C. Gessner *et al.*, "Mapping microvasculature with acoustic angiography yields quantifiable differences between healthy and in a rodent model," *Radiology*, vol. 264, no. 3, pp. 733–740, 2012.

[38] S. E. Shelton *et al.*, "Quantification of microvascular tortuosity during tumor evolution using acoustic angiography," *Ultrasound Med. Biol.*, vol. 41, no. 7, pp. 1896–1904, 2015.

[39] B. D. Lindsey *et al.*, "High resolution ultrasound superharmonic perfusion imaging: In vivo feasibility and quantification of dynamic contrast-enhanced acoustic angiography," *Ann. Biomed. Eng.*, vol. 45, pp. 939–948, 2016.

[40] S. K. Kasoji *et al.*, "Early assessment of tumor response to radiation therapy using high-resolution quantitative microvascular ultrasound imaging," *Theranostics*, vol. 8, no. 1, pp. 156–168, 2018.

[41] B. I. Rini and K. Flaherty, "Clinical effect and future considerations for molecularly-targeted therapy in renal cell carcinoma," *Urologic Oncology*, vol. 26, no. 5, pp. 543–549, 2008.

[42] R. J. Motzer *et al.*, "Activity of SU11248, a multitargeted inhibitor of vascular endothelial growth factor receptor and platelet-derived growth factor receptor, in patients with metastatic renal cell carcinoma," *J. Clin. Oncology*, vol. 24, no. 1, pp. 16–24, 2006.

[43] K. M. Cook and W. D. Figg, "Angiogenesis inhibitors: Current strategies and future prospects," *CA, Cancer J. Clin.*, vol. 60, no. 4, pp. 222–243, 2010.

[44] H. K. Gan *et al.*, "Sunitinib in solid tumors," *Expert Opinion Investigational Drugs*, vol. 18, no. 6, pp. 821–834, 2009.

[45] W. Y. Kim and W. G. Kaelin, "Molecular pathways in renal cell carcinoma: rationale for targeted treatment," *Semin. Oncology*, vol. 33, no. 5, pp. 588–595, 2006.

[46] C. J. Creighton *et al.*, "Comprehensive molecular characterization of clear cell renal cell carcinoma," *Nature*, vol. 499, no. 7456, pp. 43–49, 2013.

[47] G. Bergers and D. Hanahan, "Modes of resistance to anti-angiogenic therapy," *Nature Rev. Cancer*, vol. 8, no. 8, pp. 592–603, Aug. 2008.

[48] B. I. Rini and M. B. Atkins, "Resistance to targeted therapy in renal-cell carcinoma," *Lancet Oncology*, vol. 10, no. 10, pp. 992–1000, 2009.

[49] R. J. Motzer *et al.*, "Overall survival and updated results for sunitinib compared with interferon alfa in patients with metastatic renal cell carcinoma," *J. Clin. Oncology*, vol. 27, no. 22, pp. 3584–3590, 2009.

[50] J. C. Chappell *et al.*, "Flt-1 (vascular endothelial growth factor receptor-1) is essential for the vascular endothelial growth factor-Notch feedback loop during angiogenesis," *Arteriosclerosis, Thrombosis, Vascular Biol.*, vol. 33, no. 8, pp. 1952–1959, 2013.

[51] M. Hellström *et al.*, "Dll4 signalling through Notch1 regulates formation of tip cells during angiogenesis," *Nature*, vol. 445, no. 7129, pp. 776–780, 2007.

[52] J. C. Chappell *et al.*, "Regulation of blood vessel sprouting," *Semin. Cell Dev. Biol.*, vol. 22, no. 9, pp. 1005–1011, 2011.

[53] F. Kuhnert *et al.*, "Dll4-Notch signaling as a therapeutic target in tumor angiogenesis," *Vascular Cell*, vol. 3, no. 1, 2011, Art. no. 20.

[54] J. Ridgway *et al.*, "Inhibition of Dll4 signalling inhibits tumour growth by deregulating angiogenesis," *Nature*, vol. 444, pp. 1083–1087, 2006.

[55] I. Noguera-Troise *et al.*, "Blockade of Dll4 inhibits tumour growth by promoting non-productive angiogenesis," *Nature*, vol. 444, no. 7122, pp. 1032–1037, 2006.

[56] K. M. Miles *et al.*, "Dll4 blockade potentiates the anti-tumor effects of VEGF inhibition in renal cell carcinoma patient-derived xenografts," *PLoS One*, vol. 9, no. 11, 2014, Art. no. e112371.

[57] T. J. Czernuszewicz *et al.*, "A new preclinical ultrasound platform for widefield 3D imaging of rodents," *Rev. Sci. Instrum.*, vol. 89, 2018, Art. no. 075107.

[58] M. D. Abràmoff *et al.*, "Image processing with ImageJ," *Biophoton. Int.*, vol. 11, no. 7, pp. 36–43, 2004.

[59] F. Lin *et al.*, "3-D ultrasound localization microscopy for identifying microvascular morphology features of tumor angiogenesis at a resolution beyond the diffraction limit of conventional ultrasound," *Theranostics*, vol. 7, no. 1, pp. 196–204, 2017.

[60] C. Errico *et al.*, "Ultrafast ultrasound localization microscopy for deep super-resolution vascular imaging," *Nature*, vol. 527, no. 7579, pp. 499–502, 2015.

[61] Y. Desailly *et al.*, "Resolution limits of ultrafast ultrasound localization microscopy," *Phys. Med. Biol.*, vol. 60, no. 22, pp. 8723–8740, 2015.

[62] A. A. M. van der Veldt *et al.*, "Targeted therapies in renal cell cancer: Recent developments in imaging," *Targeted Oncology*, vol. 5, pp. 95–112, 2010.